Molecular structure of a prevalent amyloid-β fibril polymorph from Alzheimer's disease brain tissue

Ujjayini Ghosh[a,1], Kent R. Thurber[a], Wai-Ming Yau[a], and Robert Tycko[a,2]

[a]Laboratory of Chemical Physics, National Institute of Diabetes and Digestive and Kidney Diseases, NIH, Bethesda, MD 20892

This contribution is part of the special series of Inaugural Articles by members of the National Academy of Sciences elected in 2020.

Contributed by Robert Tycko, November 30, 2020 (sent for review November 6, 2020; reviewed by Ralf Langen and Sjors H. W. Scheres)

Amyloid-β (Aβ) fibrils exhibit self-propagating, molecular-level polymorphisms that may contribute to variations in clinical and pathological characteristics of Alzheimer's disease (AD). We report the molecular structure of a specific fibril polymorph, formed by 40-residue Aβ peptides (Aβ40), that is derived from cortical tissue of an AD patient by seeded fibril growth. The structure is determined from cryogenic electron microscopy (cryoEM) images, supplemented by mass-per-length (MPL) measurements and solid-state NMR (ssNMR) data. Previous ssNMR studies with multiple AD patients had identified this polymorph as the most prevalent brain-derived Aβ40 fibril polymorph from typical AD patients. The structure, which has 2.8-Å resolution according to standard criteria, differs qualitatively from all previously described Aβ fibril structures, both in its molecular conformations and its organization of cross-β subunits. Unique features include twofold screw symmetry about the fibril growth axis, despite an MPL value that indicates three Aβ40 molecules per 4.8-Å β-sheet spacing, a four-layered architecture, and fully extended conformations for molecules in the central two cross-β layers. The cryoEM density, ssNMR data, and MPL data are consistent with β-hairpin conformations for molecules in the outer cross-β layers. Knowledge of this brain-derived fibril structure may contribute to the development of structure-specific amyloid imaging agents and aggregation inhibitors with greater diagnostic and therapeutic utility.

amyloid structure | Alzheimer's disease | cryo-electron microscopy | solid-state NMR

Fibrillar assemblies formed by amyloid-β (Aβ) peptides are the primary proteinaceous component of the amyloid plaques, diffuse amyloid, and vascular amyloid in brain tissue of Alzheimer's disease (AD) patients. The most abundant forms of Aβ are 40 and 42 amino acids in length (Aβ40 and Aβ42). Mature fibrils formed by full-length Aβ peptides always contain in-register, parallel β-sheets with a cross-β orientation relative to the fibril growth direction (1–3). However, studies of Aβ fibrils grown in vitro have shown that other aspects of their molecular structures are variable (4–10). Moreover, when new Aβ fibrils are grown from fragments of existing fibrils (i.e., from fibril seeds), molecular structural differences are preserved. Thus, Aβ fibrils exhibit self-propagating, molecular-level polymorphism (4). Full molecular structural models for various Aβ40 and Aβ42 fibril polymorphs prepared in vitro have been developed from solid-state NMR (ssNMR) data (6, 7, 11–16) and from cryogenic electron microscopy (cryoEM) (17).

Evidence that structural variations in Aβ fibrils may correlate with variations in clinical and pathological characteristics of AD (18–23) provides a strong motivation for detailed structural characterization of brain-derived fibril polymorphs. Spectroscopic signatures (i.e., NMR chemical shifts) of the most common Aβ40 and Aβ42 fibril polymorphs in AD brain were identified in recent ssNMR measurements by Qiang et al. (24), in which isotopically labeled Aβ fibrils were prepared by seeded growth from cerebral cortical tissue. Based on these and other studies (25, 26), it appears that Aβ fibril polymorphs in human brain tissue are different from those that have been characterized in vitro.

Here we report the molecular structure of the Aβ40 fibril polymorph identified by Qiang et al. as the most common polymorph from AD brain (24). From a high-resolution cryoEM density map, we find that these fibrils have a four-layered cross-β structure, with twofold screw symmetry about the fibril growth direction and with fully extended conformations for Aβ40 molecules in the inner layers. Surprisingly, mass-per-length (MPL) measurements by dark-field transmission electron microscopy (TEM) of unstained samples indicate three complete Aβ40 molecules per 4.8-Å β-sheet spacing in the growth direction. We resolve the apparent contradiction between the symmetry and MPL value by proposing that the outer cross-β layers are composed of molecules with β-hairpin conformations, similar to hairpin-based cross-β structures suggested (27) and observed (28) in earlier studies of amyloid structures. The cryoEM density map and ssNMR measurements are consistent with the proposed structure, as explained below. Identification of these unanticipated molecular and supramolecular structural features in a brain-derived Aβ40 fibril polymorph may contribute to the development of fibrillation inhibitors and amyloid imaging agents with improved structural specificity, therapeutic value, and diagnostic power.

Significance

Amyloid-β (Aβ) fibrils are the main component of amyloid plaques that develop in brain tissue of Alzheimer's disease (AD) patients. Aβ fibrils have a variety of molecular structures called polymorphs. Structural variations in Aβ fibrils may contribute to variations in the severity, progression rate, or clinical manifestations of AD. Previous studies, using seeded fibril growth from human cortical tissue and solid-state nuclear magnetic resonance spectroscopy, identified a single most prevalent polymorph for 40-residue Aβ (Aβ40) fibrils in typical AD patients. Here we report the molecular structure of this most prevalent Aβ40 fibril polymorph, determined with electron microscopy methods. Unique structural features of this polymorph may allow the future development of inhibitors and imaging agents with therapeutic and diagnostic value.

Author contributions: U.G. and R.T. designed research; U.G., K.R.T., and R.T. performed research; W.-M.Y. contributed new reagents/analytic tools; U.G., K.R.T., and R.T. analyzed data; and U.G., K.R.T., and R.T. wrote the paper.

Reviewers: R.L., University of Southern California; and S.H.W.S., Medical Research Council Laboratory of Molecular Biology.

The authors declare no competing interest.

[1]Present address: Department of Chemistry, Michigan State University, East Lansing, MI 48824.

[2]To whom correspondence may be addressed. Email: robertty@mail.nih.gov.

This article contains supporting information online at https://www.pnas.org/lookup/suppl/doi:10.1073/pnas.2023089118/-/DCSupplemental.

Published January 11, 2021.

Results

Electron Microscopy of Brain-Derived Aβ40 Fibrils. Aβ40 fibrils for structural measurements by cryoEM and ssNMR were prepared by seeding solutions of synthetic or recombinant Aβ40 with sonicated fibrils that had been produced by seeded growth from cortical tissue extracts from two AD patients (*SI Appendix, Supporting Methods*). These samples are therefore "second-generation" fibrils. Negative-stain TEM and cryoEM images (Fig. 1 *A* and *B*) show that the fibrils exhibit the same modulation of their apparent widths as the first-generation, brain-seeded fibrils from which they derive (24, 25), with cross-over distances (i.e., distances between width minima) of about 120 nm (*SI Appendix*, Fig. S1 *A* and *B*). As shown previously by Ghosh et al. (29), second-generation and first-generation fibrils also have the same ssNMR spectra. Importantly, the fact that second-generation fibril samples contain less extraneous material from the original brain extracts allowed us to obtain high-quality cryoEM images, suitable for molecular structure determination.

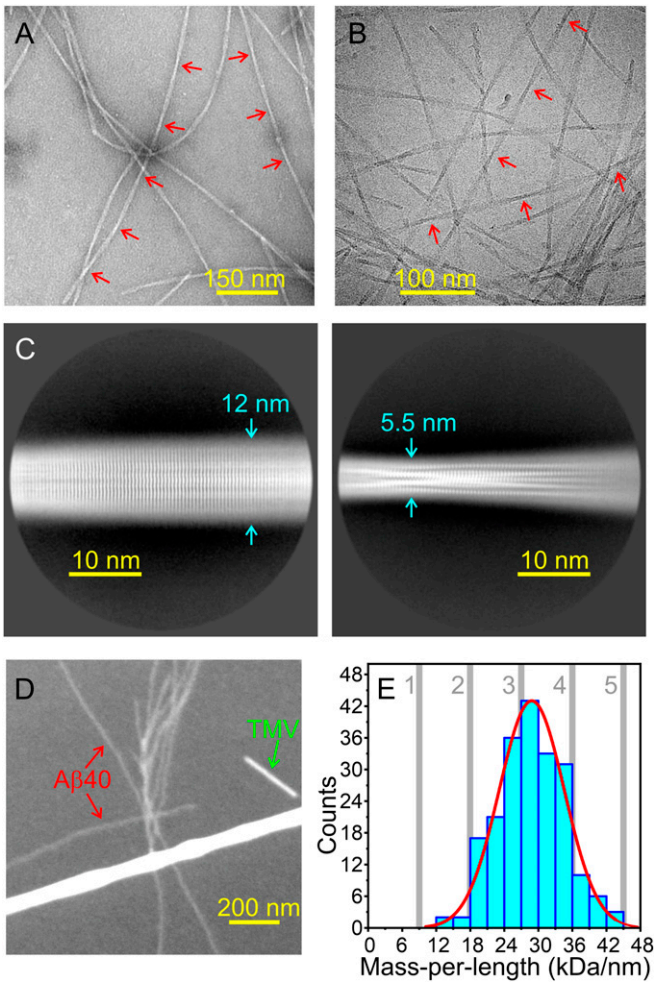

Fig. 1. Electron microscopy of brain-derived Aβ40 fibrils. (*A*) Negative-stain TEM image of second-generation fibrils used for cryoEM. Red arrows indicate approximate cross-over points. (*B*) Example of a cryoEM image, low-pass-filtered to make fibrils more readily visible. (*C*) Examples of 2D classes, generated from 241,105 particles in 1,337 cryoEM images. (*D*) Example of a dark-field TEM image of unstained third-generation fibrils. TMV rods serve as intensity standards for quantification of fibril MPL. (*E*) MPL histogram from dark-field TEM images. Vertical gray bars indicate theoretical MPL values for one to five cross-β units. A Gaussian fit centered at 28.8 kDa/nm with 13.5-kDa/nm full width at half maximum is shown in red.

To be specific, Aβ40 fibrils for cryoEM, atomic force microscopy (AFM), and MPL measurements described below were derived from parietal lobe tissue from a patient called "t-AD3" in the paper by Qiang et al. (24). Uniformly ^{15}N,^{13}C-labeled Aβ40 fibrils for ssNMR were derived from frontal lobe tissue from a patient called "patient 2" in the paper by Lu et al. (25). Aβ40 fibrils with ^{15}N and ^{13}C labels at specific backbone amide and carbonyl sites were derived from occipital lobe tissue of patient t-AD3. According to two-dimensional (2D) ^{13}C-^{13}C and ^{15}N-^{13}C ssNMR spectra of first-generation brain-seeded fibrils (24, 25), both of these patients had the same predominant Aβ40 fibril polymorph in their cortical tissue.

Fig. 1*C* shows examples of 2D class averages derived from cryoEM images. Pronounced striations perpendicular to the fibril growth direction, with a spacing of about 4.8 Å, indicate the expected cross-β structure. All 2D classes have approximate reflection symmetry with respect to their midline, indicating a structure with twofold rotational or screw symmetry about the growth direction. However, measurements of the MPL value of these fibrils, by quantification of intensities in dark-field TEM images (5, 30), yield MPL = 28.8 ± 0.4 kDa/nm (Fig. 1 *D* and *E* and *SI Appendix*, Fig. S1 *C* and *D*). Given the 4.33-kDa molecular mass of Aβ40 and the 4.8-Å cross-β spacing, an Aβ40 fibril structure consisting of two cross-β subunits with the usual in-register, parallel β-sheet organization would have MPL ≈ 18 kDa/nm, while a structure consisting of three cross-β subunits would have MPL ≈ 27 kDa/nm (4, 5, 7, 25, 30). [As amply demonstrated by MPL measurements on other amyloid-forming proteins, MPL values include both ordered and disordered segments in cross-β structures (30–32).] Thus, we encounter the conundrum of a structure that apparently contains three cross-β subunits, somehow arranged with approximate twofold symmetry about the growth direction.

Four-Layered Density Map and Molecular Structure of Inner Cross-β Layers. To derive a three-dimensional (3D) density map from the cryoEM images, we used RELION software for helical reconstruction (33, 34), modified to include correlations of particle orientations about the fibril growth direction for particles from the same fibril segment (*SI Appendix, Supporting Text*). Calculations were performed without additional symmetry, with twofold rotational symmetry in the repeat unit, and with 2_1 screw symmetry. The density map with the highest final resolution (2.77 Å) was obtained with near-2_1 symmetry, generated by a rise of 2.45 Å and twist of −180.34° between repeats (Fig. 2*A*). A density map without additional symmetry and Fourier-shell correlation plots are shown in *SI Appendix*, Fig. S2.

The density in Fig. 2*A* consists of four cross-β layers. Amino acid side chains in the two inner layers are well-resolved, allowing a unique fitting of residues 13 to 40 into the density (see *SI Appendix, Supporting Methods*). The molecular structural model shown in Fig. 2*A* was obtained by simulated annealing within Xplor-NIH software (35), including potential energy terms that represent restraints from the density map as well as backbone torsion angle restraints from ssNMR data (discussed below). In a bundle of structures from 10 independent simulated annealing calculations (*SI Appendix*, Fig. S2*C*), the rmsd among backbone atom coordinates of residues 14 to 40 was 0.37 Å. The rmsd for all coordinates of all atoms of residues 14 to 40 was 1.37 Å. Thus, the precision of this part of the structure is substantially higher than the nominal resolution of the entire density map.

In the inner cross-β layers, residues 13 to 22 form an N-terminal extended segment with one continuous β-strand. Residues 30 to 40 form a C-terminal extended segment composed of β-strands in residues 30 to 32, 34 to 36, and 38 to 39, defined by their intermolecular hydrogen bonding patterns. Glycine residues at positions 33 and 37 adopt non-β-strand conformations, disrupting these patterns. All β-strand segments

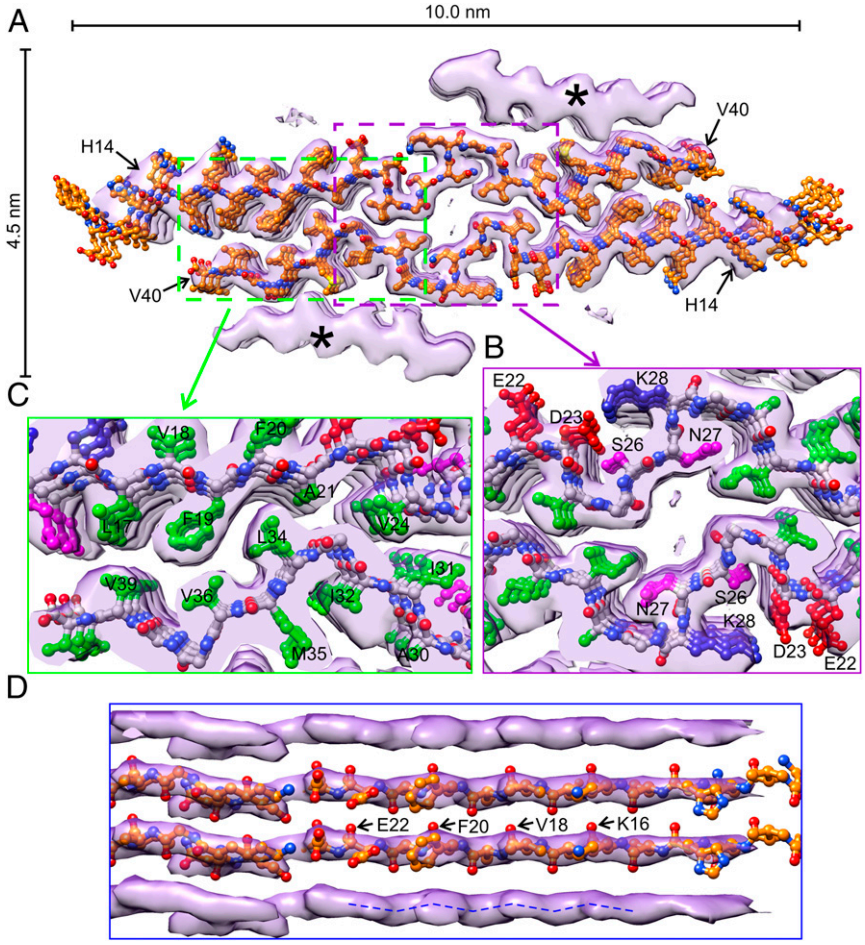

Fig. 2. Density map and molecular model for brain-derived Aβ40 fibrils. (*A*) Cross-sectional view of the full density with three repeats of the molecular model for residues 10 to 40 in the inner cross-β layers. All carbon atoms are shown in orange. Hydrogen atoms are omitted. The density has near 2_1 symmetry, with a slight left-handed twist. (*B*) Expanded view of the central pore, showing D23–K28 salt bridge interactions. Carbon atoms of amino acid side chains are green (hydrophobic), magenta (polar), blue (positively charged), or red (negatively charged). (*C*) Expanded view of hydrophobic interactions between the inner layers. (*D*) Lateral view of the β-sheet formed by residues 14 to 22. Alignment of backbone density corrugations (dashed blue line) with backbone carbonyl directions favors the left-handed density over its right-handed mirror image.

in the inner layers participate in in-register parallel β-sheets. The N-terminal and C-terminal extended segments are separated by an irregular conformation in central residues 23 to 29, apparently stabilized in part by electrostatic interactions involving oppositely charged side chains of D23 and K28 (Fig. 2*B*). Residues 1 to 12 are not sufficiently ordered to contribute to the density.

Conformations within N-terminal, central, and C-terminal segments in Fig. 2*A* resemble conformations of the same segments in previously described Aβ fibril structures (6, 14, 25), but the overall structural arrangement is qualitatively different. In previous structures, non-β-strand conformations at certain residues allow each Aβ molecule to fold onto itself, resulting in roughly U-shaped (6, 7, 11, 25), S-shaped (12, 13, 15–17), or C-shaped (14, 26) conformations that are stabilized by interactions among hydrophobic side chains within a single cross-β subunit. In contrast, each Aβ40 molecule in the inner layers in Fig. 2*A* remains nearly fully extended. Hydrophobic interactions are then exclusively between different cross-β subunits (i.e., different layers of molecules) as shown in Fig. 2*C*.

The density map in Fig. 2*A* has a gradual left-handed twist. CryoEM images are invariant to a reflection of the molecular structure, implying that a mirror-image density with a right-handed twist must fit the images equally well. Fig. 2*D* shows that the left-handed backbone density corrugations match backbone carbonyl directions in our structural model, while corrugations in the mirror-image density (*SI Appendix*, Fig. S3 *A* and *B*) clash with backbone carbonyl directions. AFM images also support a left-handed twist (*SI Appendix*, Fig. S3*C*).

Proposal of β-Hairpins in Outer Cross-β Layers. The inner layers in the density map for our brain-derived Aβ40 fibrils account for 18 kDa/nm of MPL. We propose that the remaining MPL contribution comes from the two outer layers (asterisks in Fig. 2*A*), implying that each outer layer contributes about 5 kDa/nm to the MPL. The outer layers appear to be cross-β motifs, composed of β-strands that are eight or nine residues in length, with clear separations along the fibril growth direction. What could the molecular structure in the outer layers be?

One possibility is that the outer layers are cross-β motifs with the usual 4.8-Å intermolecular spacing, but with ~50% occupancy and with only one β-strand segment per molecule. However, the magnitude of the density in the outer layers equals that in the inner layers, ruling out partial occupancy (*SI Appendix*, Fig. S4). A second possibility, that the outer layers are density from residues 1 to 12 of Aβ40 molecules in the inner layers, is inconsistent with the MPL data. Structural modeling also rules out this possibility, because the outer layers are too far from residue H13 (*SI Appendix*, Fig. S5).

A third possibility is that the outer layers are cross-β motifs constructed from β-hairpins, resembling structures in fibrils formed by certain designed peptides (28). In this context, it is worth noting that Aβ peptides adopt β-hairpin conformations in affibody complexes (36), that Aβ peptides constrained to β-hairpin conformations by intramolecular disulfide bridges form oligomers and protofibrils (37), that macrocyclic β-hairpin peptides based on Aβ form compact oligomers (38), that β-hairpin conformations are sampled in computational studies of Aβ monomers (39), and that an early model for Aβ fibril structures was based on β-hairpin conformations (27). As depicted in Fig. 3*A*, a variety of β-hairpin structures is conceivable, all of which would contribute about 4.5 kDa/nm to the MPL.

Fig. 3*B* shows one specific model, in which residues 15 to 22 and 30 to 37 form β-strands that participate in both intramolecular and intermolecular backbone hydrogen bonds, and residues 23 to 29 form turns that lie above or below the C termini of molecules in the inner layers. Since a fully ordered structure of this type would have a repeat distance of 9.6 Å (or 9.8 Å, based on the 2.45-Å rise of the final density map with 2_1 symmetry), densities from the two different β-strand segments of the β-hairpins would be averaged together in Fig. 2*A*, consistent with the poorly defined side chains of the outer layers. Attempts to process the cryoEM images with rise values around 9.8 Å did not improve the resolution of these side chains. However, different fibril segments could contain different β-hairpin-like structures in their outer layers, or different alignments of the β-hairpins between the two outer layers, with only minor effects on the molecular structure of the inner layers. Such disorder in the outer layers would preclude higher resolution.

One might expect a 9.8-Å repeat distance in the outer cross-β layers to become visible in 2D Fourier transforms (FTs) of fibrils from the cryoEM images, averaged over many particle boxes after taking the magnitude of the FT of each particle. As shown in *SI Appendix*, Fig. S6, a weak feature that may represent 9.8-Å periodicity does occur in the average FTs of particle boxes from the experimental images. Simulated images from structural models that include β-hairpin conformations in the outer layers, and also include the disordered N-terminal and C-terminal tails of all Aβ40 molecules, lead to average FTs with 9.8-Å features that are comparable in magnitude to the 9.8-Å features in the average FTs from the experimental images (*SI Appendix*, Fig. S6 and *Supporting Methods*). Additional disorder or defects in the outer layers would further weaken the 9.8-Å feature.

Interestingly, 2D projections calculated from models with two different orientations for β-hairpins in the outer layers are noticeably different (*SI Appendix*, Fig. S6*B*). Projections calculated from a model in which residues 23 to 29 in the outer layers, representing the turns in the β-hairpins, lie above or below the C termini of molecules in the inner layers, are in good agreement with the 2D class images obtained from the experimental cryoEM images. Projections calculated from a model with the opposite orientation of the β-hairpins (i.e., with residues 23 to 29 of molecules in the outer layers lying above or below K29 residues of the inner layers) show somewhat poorer agreement with the 2D class images. Also, the simulated density map from the former model agrees more closely with the experimental density map (*SI Appendix*, Figs. S4*A* and S6*A*). Therefore, we favor an orientation of β-hairpins in the outer cross-β layers that places their turn segments in close proximity to the C termini of molecules in the inner layers.

Support from ssNMR Data. ssNMR measurements, performed on uniformly ^{15}N,^{13}C-labeled second-generation fibrils, support the molecular model. From 2D and 3D ssNMR spectra (Fig. 4*A* and *SI Appendix*, Figs. S7 and S8), we obtained ^{15}N and ^{13}C chemical shift assignments for residues 16 to 25 and 27 to 37 (*SI Appendix*, Table S1). Predictions of backbone ϕ and ψ torsion angles based on these chemical shifts (40) are fully consistent with the cryoEM density map (Fig. 4 *B* and *C*). Torsion angle restraints from

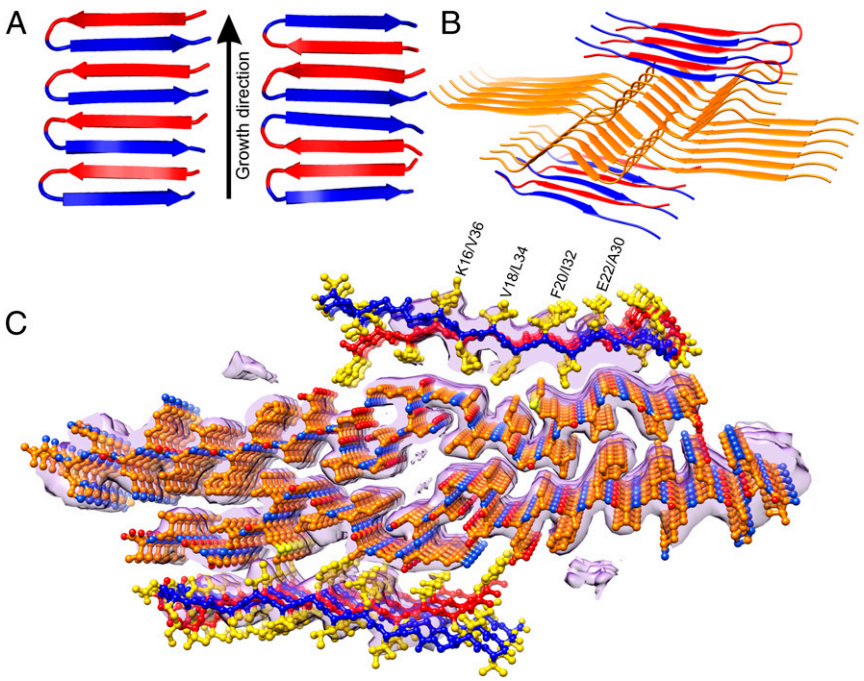

Fig. 3. Proposed model for the outer cross-β layers of brain-derived Aβ40 fibrils. (*A*) Two examples of cross-β motifs composed of β-hairpins. Any such motif would contribute 4.5 kDa/nm to the experimentally measured MPL value. (*B*) Ribbon representation of one possibility for the full fibril structure, omitting disordered N-terminal tail segments. Such a structure would have MPL ≈ 27 kDa/nm and would fill the cryoEM density. (*C*) Atomic representation of the same possible structure. In the outer layers, backbone atoms of residues 13 to 26 and 27 to 40 are red and blue, respectively. Side-chain atoms are yellow.

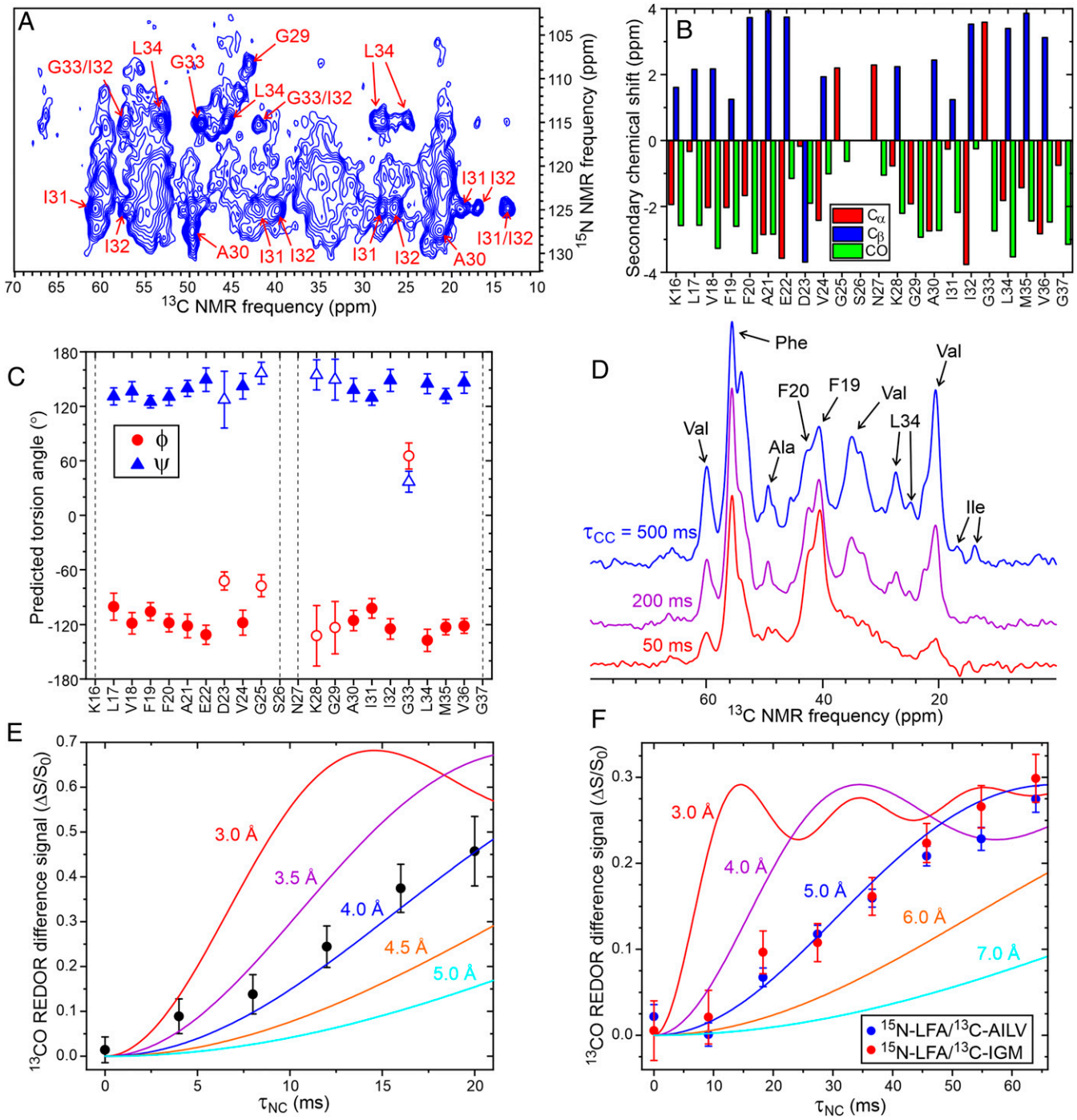

Fig. 4. ssNMR data for brain-derived Aβ40 fibrils. (*A*) Two-dimensional NCACX spectrum of second-generation fibrils with uniform ^{15}N and ^{13}C labeling. Residue-specific assignments for strong, sharp cross-peaks are shown. Contour levels increase by successive factors of 1.25. (*B*) Secondary ^{13}C chemical shifts determined from 2D and 3D spectra. (*C*) Backbone ϕ and ψ torsion angle predictions from ^{15}N and ^{13}C chemical shifts. Predictions classified as "strong" by the TALOS-N program are shown in filled symbols. (*D*) Aliphatic region of the ^{13}C ssNMR spectrum, showing the dependence on the ^{13}C-^{13}C polarization transfer period τ_{CC} after selective excitation of aromatic ^{13}C polarization. (*E*) Dependence of the fsREDOR difference signal from the side-chain carboxyl site of D23 on the ^{15}N-^{13}C dipolar dephasing period τ_{NC}. Color-coded lines are simulations for dipole-coupled ^{15}N/^{13}C spin pairs with the indicated interatomic distances. (*F*) REDOR data for fibrils that were ^{15}N-labeled at backbone amide sites of L17, F19, and A21 and ^{13}C-labeled at backbone carbonyl sites of A30, I32, L34, and V36 (blue symbols) or I31, G33, and M35 (red symbols). Comparisons with simulations support an average ^{15}N-^{13}C distance of about 5 Å for one-third of the Aβ40 molecules, consistent with a β-hairpin-like structure in the outer layers of the cryoEM density.

ssNMR were included in calculations of a structure bundle by simulated annealing (35). As mentioned above, the conformation of residues 14 to 40 in this bundle is quite well defined (*SI Appendix*, Fig. S2*C*), with rmsd values of 0.37 Å for backbone atoms and 1.37 Å for all atoms.

Two-dimensional and 3D ssNMR spectra also contain unassigned signals that may arise from molecules in the outer cross-β layers of the density map (*SI Appendix*, Figs. S7*A* and S8). Compared to the corresponding spectra of Aβ40 and Aβ42 fibrils in which all molecules are equivalent by symmetry (13–15, 17,

25), 2D and 3D ssNMR spectra of the brain-derived Aβ40 fibrils discussed here exhibit relatively broad cross-peaks, despite the fact that the fibrils are morphologically homogeneous in negative-stain TEM and cryoEM images. Greater spectral congestion and broader lines are consistent with the coexistence of structural order in the inner layers with inequivalent molecular conformations and greater disorder in the outer layers. Even a structure with perfectly ordered β-hairpins in the outer layers, as depicted in Fig. 3*C*, would necessarily contain three structurally inequivalent molecules in the repeat unit (i.e., two in the inner layers and one in the outer layers).

Interresidue ^{13}C-^{13}C polarization transfers, observed in one-dimensional ^{13}C spectra after selective excitation of aromatic ^{13}C polarization (Fig. 4*D* and *SI Appendix*, Fig. S9) or in 2D ^{13}C-^{13}C spectra with a 500-ms mixing period (*SI Appendix*, Fig. S7*C*), indicate contacts between the L34 side chain and a phenylalanine side chain (most likely F19), as in Fig. 2*C*. Measurements of ^{15}N-^{13}C dipole–dipole couplings with the frequency-selective rotational echo double-resonance (fsREDOR) technique (41) indicate a distance of 3.8 ± 0.2 Å between C_γ of D23 and N_ε of K28 (Fig. 4*E*), consistent with the D23–K28 salt bridges in Fig. 2*B*.

Finally, as a test for β-hairpin-like structures in the outer layers of the density map, we prepared second-generation Aβ40 fibrils with ^{15}N labels at backbone amide sites of L17, F19, and A21 and ^{13}C labels at backbone carbonyl sites of either A30, I32, L34, and V36 or I31, G33, and M35. With these labeling patterns, the shortest ^{15}N-^{13}C distances within the inner cross-β layers are either 6.5 Å or 8.5 Å (^{15}N-A21 to ^{13}CO-G33 or ^{15}N-A21 to ^{13}CO-L34 between layers). In contrast, ^{15}N-^{13}C distances in the 4- to 6-Å range may occur in a cross-β motif composed of β-hairpins (*SI Appendix*, Fig. S10). As shown in Fig. 4*F*, REDOR measurements (42) on both selectively labeled fibril samples indicate ^{15}N-^{13}C couplings that are consistent with an average distance of 5.1 ± 0.3 Å for the carbonyl ^{13}C labels in one-third of the Aβ40 molecules.

Discussion

Relation to Other Brain-Derived Aβ40 Fibril Structures. Two other brain-derived Aβ40 fibril structures have been described previously. Using ssNMR, Lu et al. developed a structural model for brain-derived fibrils with MPL ~ 27 kDa/nm but which were otherwise quite different from the fibrils discussed above (25). In particular, the fibrils studied by Lu et al. (25) had a rod-like morphology, without width modulation in TEM images, and exhibited a single set of strong, sharp ssNMR signals for residues 1 to 40, indicating threefold symmetry about the fibril growth axis (*SI Appendix*, Fig. S11*A*). The same polymorph was not detected in subsequent measurements by Qiang et al. (24), demonstrating that this was a rare polymorph, consistent with the atypical clinical history of the AD patient (called "patient 1") from which it was derived (25). Using cryoEM, Kollmer et al. developed a structural model for Aβ40 fibrils isolated from meninges (26). Unlike the cerebral cortex-derived fibrils discussed above, the fibrils from meninges exhibited a right-handed twist, with a cross-over distance of about 40 nm. In the model developed by Kollmer et al. (26), residues 1 to 35 are contained within the cryoEM density and the C terminus of Aβ40 may also be structurally ordered (*SI Appendix*, Fig. S11*B*). D23–K28 salt bridges and F19–L34 hydrophobic contacts are absent. Although in certain respects the density map obtained by Kollmer et al. (26) resembles the density map in Fig. 2*A*, it is not identical (*SI Appendix*, Fig. S11*C*).

Essential Nature of the Outer Cross-β Layers. In a recent cryoEM study of TDP-43 fibrils by Cao et al. (43), extra density that resembles the outer cross-β layers discussed above was interpreted as evidence for ongoing secondary nucleation, that is, seeding of new fibrils along the sides of existing fibrils (44). In the case of our brain-derived Aβ40 fibrils, we interpret the outer layers as essential components of the fibril structure, not as incipient new fibrils. Our interpretation is supported by the full occupancy of these layers (*SI Appendix*, Fig. S4). In addition, dark-field TEM images obtained at various time points during fibril growth indicate a constant MPL value (*SI Appendix*, Fig. S12). The MPL data show no evidence for a gradual build-up of the outer layers as fibril growth proceeds, nor for a gradual loss of the outer layers at long incubation times or after dilution of the fibrils into fresh buffer.

We cannot exclude the possibility that Aβ40 molecules in the outer layers are less tightly bound to the fibril structure than molecules in the inner layers. It is conceivable that molecules or groups of molecules in the outer layers could dissociate from the fibril as part of a secondary nucleation process and then be replaced by other Aβ40 molecules. Additional experiments would be required to determine whether such a process occurs and, if so, the relevant kinetic parameters.

Validity of Seeded Fibril Growth as an Approach to Structures of Brain-Derived Amyloid Fibrils. Our use of seeded fibril growth allows us to obtain brain-derived Aβ40 fibril samples that are largely devoid of extraneous material from the cortical tissue, which facilitates high-resolution structure determination by cryoEM. Fibrils prepared by seeded growth also occur primarily as single filaments in the cryoEM, TEM, and AFM images, which is another important factor in the success of the experiments described above. This approach depends on faithful propagation of molecular structures in seeded fibril growth, which we have demonstrated in previous ssNMR studies of Aβ40 fibrils (4, 25, 29). We have also shown that multiple rounds of seeded growth can alter the relative populations of different polymorphs that are present in a heterogeneous initial sample, selectively amplifying polymorphs that propagate more efficiently than others under a specific seeded growth protocol (7, 45). In order to minimize the possibility of selective amplification of specific polymorphs in the brain tissue, the first-generation fibrils in experiments described above were prepared with a single seeding step, by adding soluble Aβ40 to sonicated tissue extract only once (24, 25). Faithful propagation of molecular structures in subsequent generations has been verified by ssNMR measurements on the brain-derived fibrils (25, 29).

It should be emphasized that the cortical tissue extract used to prepare first-generation fibrils was prepared with a gentle protocol that is expected to preserve all fibril polymorphs (25). We do not use a rigorous purification of amyloid from the tissue. Amyloid in the extract represents less than 1% of the total material, with the remainder being other components of the homogenized tissue. With suitable control experiments, we have shown previously that seeded Aβ40 fibril growth comes from the amyloid in the extract, not from other components (24, 25).

An alternative approach would be to isolate fibrils from the tissue and examine the fibrils directly by cryoEM, without amplification by seeded growth. In principle, this approach would avoid uncertainties regarding faithful structure propagation in the first generation. However, this approach requires a more extensive purification of the fibrils, which has the potential to alter fibril structures or select specific polymorphs that may not be representative of the predominant polymorphs in the original tissue.

Successful cryoEM studies of amyloid fibrils isolated from human brain tissue, without amplification, have been reported by Scheres, Goedert, and coworkers in the case of tau fibrils (46–49) and α-synuclein fibrils (50). These studies used sarcosyl detergent, repeated centrifugations, and in some cases pronase digestion (48, 49) to prepare clean, well-separated fibrils suitable for cryoEM. It is unclear whether the same protocols would be

sufficient to isolate Aβ fibrils from cortical tissue in a state suitable for high-resolution cryoEM. The studies of meningeal Aβ40 fibrils by Kollmer et al. (26) also did not use amplification by seeded growth. The specific properties of meninges allowed fibrils to be isolated without detergents or other harsh treatments. Our own previous attempts to purify Aβ fibrils from cortical tissue, using sodium dodecyl sulfate detergent treatment, sucrose gradient centrifugations, and enzymatic digestion of collagen and DNA, resulted in fibrils that were self-associated and coated with extraneous material [see figure 1 of Paravastu et al. (51)].

In our opinion, both approaches to cryoEM studies of brain-derived amyloid fibrils are valid. Both also have their own uncertainties. Although seeded growth can faithfully propagate molecular structures (4, 25, 29), fibril structures that depend on cofactors in brain tissue may conceivably be altered when seeded growth is performed in a simple aqueous buffer. Cross-seeding between Aβ40 fibrils and Aβ42 fibrils may also complicate the interpretation of seeded structures, although seeding of Aβ40 by Aβ42 fibrils has been shown to be inefficient (12, 52). On the other hand, isolation of clean, well-separated fibrils from brain tissue without seeded growth may not be possible in all cases without treatments that select specific structures (i.e., structures that are least prone to self-association or association with other tissue components) or alter the fibril structures by removal of cofactors or by partial dissolution or digestion.

Concluding Remarks

The cryoEM, MPL, and ssNMR data described above provide evidence for an Aβ40 fibril polymorph with unanticipated structural characteristics. Aβ40 molecules in the central cross-β layers participate in the expected in-register parallel β-sheets (1–3) but have extended conformations that differ qualitatively from the U-shaped (6, 7, 11, 25), S-shaped (12, 13, 15–17), and C-shaped (14, 26) conformations in previously reported structural models for other polymorphs. The outer cross-β layers appear to be formed by Aβ40 molecules with β-hairpin conformations. Although details of the outer layer structure cannot be determined from the cryoEM density map, a cross-β structure composed of β-hairpins (27, 28) is supported by the density map, by the MPL value, and by ssNMR measurements of ^{15}N-^{13}C dipole–dipole couplings in selectively labeled samples. Aβ fibril polymorphs that contain two strongly inequivalent molecular

Table 1. Parameters for cryoEM data collection, 3D density map reconstruction, and molecular model development

Data collection	
Magnification	130,000×
Voltage	300 kV
Defocus range	−0.5 μm to −3.0 μm
Microscope	Krios
Camera	K2 Summit
Exposure time	10 s
No. of movie frames	50
Total electron dose	73.5 e/Å^2
Pixel size	1.08 Å (binned from 0.54 Å)
No. of images used	1,337
3D density map reconstruction (EMDB-21501)	
Box size (pixel)	400 pixels, 432 Å
Interbox distance	29 Å
No. of fibril segments selected	19790
No. of particles extracted from images	383,717
No. of particles after 2D classification	239,937
No. of particles in final density map	103,462
Resolution	2.77 Å
B-factor	−46.9 Å^2
Helical rise	2.45 Å
Helical twist	179.66°
Symmetry	Effectively 2_1 screw symmetry
Atomic model (PDB ID code 6W0O)	
No. of unique nonhydrogen atoms (residues 10 to 40)	234 per molecule
Rmsd of bonds	0.01 Å
Rmsd of angles	1.55°
Molprobity clash score	0.72
Favored rotamers	95%
Ramachandran outliers	0%
Ramachandran favored	95%
Xplor-NIH statistics	
No. of structures in final round of calculations	60
Total no. of violations of ANGL, BOND, CDIH, IMPR, repel, and repel14 terms in final structure bundle	0
Potential energy range of 30 lowest-energy structures (arbitrary units)	10,025.86–10,299.90
All-atom rmsd for residues 14 to 40 of central molecules in final structure bundle	1.35 Å
Backbone rmsd for residues 14 to 40 of central molecules in final structure bundle	0.37 Å

conformations and two different cross-β motifs have not been reported previously.

This brain-derived Aβ40 fibril polymorph has been shown to be prevalent in the cerebral cortex of typical AD patients (24). Thus, the molecular structure in Fig. 2 may be useful as a guide for the development of amyloid imaging agents with improved specificity and diagnostic utility. The pronounced structural differences among Aβ40 polymorphs may allow the development of structurally specific aggregation inhibitors (53) and antibodies (54), targeting polymorphs with the greatest relevance to AD.

Materials and Methods

Preparation of first-generation Aβ40 fibrils, seeded with sonicated cortical tissue extracts, was described in earlier publications (24, 25). Second- and third-generation fibrils were prepared by adding Aβ40, dissolved at high concentration in dimethyl sulfoxide, to sonicated fibrils from the previous generation in 10 mM sodium phosphate buffer, pH 7.4. Fibril growth proceeded quiescently at 24 °C. CryoEM images were recorded with conditions summarized in Table 1 and were processed as described in *SI Appendix, Supporting Text*. Dark-field TEM images of unstained samples were obtained with an FEI Morgagni microscope and analyzed as previously described (30). ssNMR data were acquired at 14.1 T and 17.5 T, using Varian InfinityPlus spectrometers and 1.8-mm magic-angle spinning probes produced by the laboratory of Ago Samoson (Tallinn University of Technology, Estonia). Full details of sample preparations, cryoEM, TEM, AFM, and ssNMR measurements, data analyses, and molecular model development are given in *SI Appendix, Supporting Methods*.

Data Availability. The final cryoEM density map is available from the Electron Microscopy Data Bank (code 21501). The final bundle of molecular models is available from the Protein Data Bank (ID code 6W0O). NMR chemical shifts are available from the Biological Magnetic Resonance Bank (code 30731). Modified RELION 3.0-beta software and associated MATLAB scripts are available upon request from K.R.T. (thurberk@niddk.nih.gov) and can be downloaded from Mendeley Data (http://doi.org/10.17632/sv77pxn7p3.1).

ACKNOWLEDGMENTS. This work was supported by the Intramural Research Program of the National Institute of Diabetes and Digestive and Kidney Diseases, NIH. CryoEM measurements were performed at the NIH Multi-Institute CryoEM Facility. Calculations of density maps and molecular models used the computational resources of the NIH High Performance Computing Biowulf cluster. We thank Drs. Jenny Hinshaw and Bertram Canagarajah for generous assistance and advice.

1. T. L. S. Benzinger *et al*., Propagating structure of Alzheimer's β-amyloid(10-35) is parallel β-sheet with residues in exact register. *Proc. Natl. Acad. Sci. U.S.A.* **95**, 13407–13412 (1998).
2. O. N. Antzutkin *et al*., Multiple quantum solid-state NMR indicates a parallel, not antiparallel, organization of β-sheets in Alzheimer's β-amyloid fibrils. *Proc. Natl. Acad. Sci. U.S.A.* **97**, 13045–13050 (2000).
3. M. Török *et al*., Structural and dynamic features of Alzheimer's Abeta peptide in amyloid fibrils studied by site-directed spin labeling. *J. Biol. Chem.* **277**, 40810–40815 (2002).
4. A. T. Petkova *et al*., Self-propagating, molecular-level polymorphism in Alzheimer's β-amyloid fibrils. *Science* **307**, 262–265 (2005).
5. C. Goldsbury, P. Frey, V. Olivieri, U. Aebi, S. A. Müller, Multiple assembly pathways underlie amyloid-β fibril polymorphisms. *J. Mol. Biol.* **352**, 282–298 (2005).
6. A. T. Petkova, W. M. Yau, R. Tycko, Experimental constraints on quaternary structure in Alzheimer's β-amyloid fibrils. *Biochemistry* **45**, 498–512 (2006).
7. A. K. Paravastu, R. D. Leapman, W. M. Yau, R. Tycko, Molecular structural basis for polymorphism in Alzheimer's β-amyloid fibrils. *Proc. Natl. Acad. Sci. U.S.A.* **105**, 18349–18354 (2008).
8. R. Kodali, A. D. Williams, S. Chemuru, R. Wetzel, Abeta(1-40) forms five distinct amyloid structures whose β-sheet contents and fibril stabilities are correlated. *J. Mol. Biol.* **401**, 503–517 (2010).
9. J. Meinhardt, C. Sachse, P. Hortschansky, N. Grigorieff, M. Fändrich, Abeta(1-40) fibril polymorphism implies diverse interaction patterns in amyloid fibrils. *J. Mol. Biol.* **386**, 869–877 (2009).
10. M. R. Elkins *et al*., Structural polymorphism of Alzheimer's β-amyloid fibrils as controlled by an E22 switch: A solid-state NMR study. *J. Am. Chem. Soc.* **138**, 9840–9852 (2016).
11. I. Bertini, L. Gonnelli, C. Luchinat, J. Mao, A. Nesi, A new structural model of Aβ40 fibrils. *J. Am. Chem. Soc.* **133**, 16013–16022 (2011).
12. Y. Xiao *et al*., Aβ(1-42) fibril structure illuminates self-recognition and replication of amyloid in Alzheimer's disease. *Nat. Struct. Mol. Biol.* **22**, 499–505 (2015).
13. M. T. Colvin *et al*., Atomic resolution structure of monomorphic Aβ(42) amyloid fibrils. *J. Am. Chem. Soc.* **138**, 9663–9674 (2016).
14. A. K. Schutz *et al*., Atomic-resolution three-dimensional structure of amyloid β fibrils bearing the Osaka mutation. *Angew. Chem. Int. Ed. Engl.* **54**, 331–335 (2015).
15. M. A. Wälti *et al*., Atomic-resolution structure of a disease-relevant Aβ(1-42) amyloid fibril. *Proc. Natl. Acad. Sci. U.S.A.* **113**, E4976–E4984 (2016).
16. Z. W. Hu *et al*., Molecular structure of an N-terminal phosphorylated β-amyloid fibril. *Proc. Natl. Acad. Sci. U.S.A.* **116**, 11253–11258 (2019).
17. L. Gremer *et al*., Fibril structure of amyloid-β(1-42) by cryo-electron microscopy. *Science* **358**, 116–119 (2017).
18. M. Meyer-Luehmann *et al*., Exogenous induction of cerebral β-amyloidogenesis is governed by agent and host. *Science* **313**, 1781–1784 (2006).
19. J. C. Watts *et al*., Serial propagation of distinct strains of Aβ prions from Alzheimer's disease patients. *Proc. Natl. Acad. Sci. U.S.A.* **111**, 10323–10328 (2014).
20. M. L. Cohen *et al*., Rapidly progressive Alzheimer's disease features distinct structures of amyloid-β. *Brain* **138**, 1009–1022 (2015).
21. J. Rasmussen *et al*., Amyloid polymorphisms constitute distinct clouds of conformational variants in different etiological subtypes of Alzheimer's disease. *Proc. Natl. Acad. Sci. U.S.A.* **114**, 13018–13023 (2017).
22. C. Condello *et al*., Structural heterogeneity and intersubject variability of Aβ in familial and sporadic Alzheimer's disease. *Proc. Natl. Acad. Sci. U.S.A.* **115**, E782–E791 (2018).
23. G. Di Fede *et al*., Molecular subtypes of Alzheimer's disease. *Sci. Rep.* **8**, 3269 (2018).
24. W. Qiang, W. M. Yau, J. X. Lu, J. Collinge, R. Tycko, Structural variation in amyloid-β fibrils from Alzheimer's disease clinical subtypes. *Nature* **541**, 217–221 (2017).
25. J. X. Lu *et al*., Molecular structure of β-amyloid fibrils in Alzheimer's disease brain tissue. *Cell* **154**, 1257–1268 (2013).
26. M. Kollmer *et al*., Cryo-EM structure and polymorphism of Aβ amyloid fibrils purified from Alzheimer's brain tissue. *Nat. Commun.* **10**, 4760 (2019).
27. L. Li, T. A. Darden, L. Bartolotti, D. Kominos, L. G. Pedersen, An atomic model for the pleated β-sheet structure of Abeta amyloid protofilaments. *Biophys. J.* **76**, 2871–2878 (1999).
28. K. Nagy-Smith, E. Moore, J. Schneider, R. Tycko, Molecular structure of monomorphic peptide fibrils within a kinetically trapped hydrogel network. *Proc. Natl. Acad. Sci. U.S.A.* **112**, 9816–9821 (2015).
29. U. Ghosh, W. M. Yau, R. Tycko, Coexisting order and disorder within a common 40-residue amyloid-β fibril structure in Alzheimer's disease brain tissue. *Chem. Commun. (Camb.)* **54**, 5070–5073 (2018).
30. B. Chen, K. R. Thurber, F. Shewmaker, R. B. Wickner, R. Tycko, Measurement of amyloid fibril mass-per-length by tilted-beam transmission electron microscopy. *Proc. Natl. Acad. Sci. U.S.A.* **106**, 14339–14344 (2009).
31. D. T. Murray *et al*., Structure of FUS protein fibrils and its relevance to self-assembly and phase separation of low-complexity domains. *Cell* **171**, 615–627.e16 (2017).
32. D. T. Murray *et al*., Structural characterization of the D290V mutation site in hnRNPA2 low-complexity-domain polymers. *Proc. Natl. Acad. Sci. U.S.A.* **115**, E9782–E9791 (2018).
33. S. H. W. Scheres, RELION: Implementation of a Bayesian approach to cryo-EM structure determination. *J. Struct. Biol.* **180**, 519–530 (2012).
34. S. He, S. H. W. Scheres, Helical reconstruction in RELION. *J. Struct. Biol.* **198**, 163–176 (2017).
35. C. D. Schwieters, J. J. Kuszewski, G. M. Clore, Using Xplor-NIH for NMR molecular structure determination. *Prog. Nucl. Magn. Reson. Spectrosc.* **48**, 47–62 (2006).
36. W. Hoyer, C. Grönwall, A. Jonsson, S. Ståhl, T. Härd, Stabilization of a β-hairpin in monomeric Alzheimer's amyloid-β peptide inhibits amyloid formation. *Proc. Natl. Acad. Sci. U.S.A.* **105**, 5099–5104 (2008).
37. A. Sandberg *et al*., Stabilization of neurotoxic Alzheimer amyloid-β oligomers by protein engineering. *Proc. Natl. Acad. Sci. U.S.A.* **107**, 15595–15600 (2010).
38. A. G. Kreutzer, J. S. Nowick, Elucidating the structures of amyloid oligomers with macrocyclic β-hairpin peptides: Insights into Alzheimer's disease and other amyloid diseases. *Acc. Chem. Res.* **51**, 706–718 (2018).
39. M. Carballo-Pacheco, B. Strodel, Comparison of force fields for Alzheimer's A β42: A case study for intrinsically disordered proteins. *Protein Sci.* **26**, 174–185 (2017).
40. Y. Shen, A. Bax, Protein backbone and sidechain torsion angles predicted from NMR chemical shifts using artificial neural networks. *J. Biomol. NMR* **56**, 227–241 (2013).
41. C. P. Jaroniec, B. A. Tounge, J. Herzfeld, R. G. Griffin, Frequency selective heteronuclear dipolar recoupling in rotating solids: Accurate $(^{13})$C-$(^{15})$N distance measurements in uniformly $(^{13})$C,$(^{15})$N-labeled peptides. *J. Am. Chem. Soc.* **123**, 3507–3519 (2001).
42. R. C. Anderson *et al*., Conformation of 1-^{13}C,^{15}N acetyl-L-carnitine: Rotational-echo, double-resonance nuclear magnetic resonance spectroscopy. *J. Am. Chem. Soc.* **117**, 10546–10550 (1995).
43. Q. Cao, D. R. Boyer, M. R. Sawaya, P. Ge, D. S. Eisenberg, Cryo-EM structures of four polymorphic TDP-43 amyloid cores. *Nat. Struct. Mol. Biol.* **26**, 619–627 (2019).
44. S. I. A. Cohen *et al*., Proliferation of amyloid-β42 aggregates occurs through a secondary nucleation mechanism. *Proc. Natl. Acad. Sci. U.S.A.* **110**, 9758–9763 (2013).

45. W. Qiang, W. M. Yau, R. Tycko, Structural evolution of Iowa mutant β-amyloid fibrils from polymorphic to homogeneous states under repeated seeded growth. *J. Am. Chem. Soc.* **133**, 4018–4029 (2011).
46. W. Zhang *et al*., Novel tau filament fold in corticobasal degeneration. *Nature* **580**, 283–287 (2020).
47. B. Falcon *et al*., Novel tau filament fold in chronic traumatic encephalopathy encloses hydrophobic molecules. *Nature* **568**, 420–423 (2019).
48. B. Falcon *et al*., Structures of filaments from Pick's disease reveal a novel tau protein fold. *Nature* **561**, 137–140 (2018).
49. A. W. P. Fitzpatrick *et al*., Cryo-EM structures of tau filaments from Alzheimer's disease. *Nature* **547**, 185–190 (2017).
50. M. Schweighauser *et al*., Structures of α-synuclein filaments from multiple system atrophy. *Nature* **585**, 464–469 (2020).
51. A. K. Paravastu, I. Qahwash, R. D. Leapman, S. C. Meredith, R. Tycko, Seeded growth of β-amyloid fibrils from Alzheimer's brain-derived fibrils produces a distinct fibril structure. *Proc. Natl. Acad. Sci. U.S.A.* **106**, 7443–7448 (2009).
52. W. M. Yau, R. Tycko, Depletion of amyloid-β peptides from solution by sequestration within fibril-seeded hydrogels. *Protein Sci.* **27**, 1218–1230 (2018).
53. Q. Cheng, W. Qiang, Solid-state NMR structure-based inhibitor design to achieve selective inhibition of the parallel-in-register β-sheet versus antiparallel Iowa mutant β-amyloid fibrils. *J. Phys. Chem. B* **121**, 5544–5552 (2017).
54. A. Hatami, R. Albay, 3rd, S. Monjazeb, S. Milton, C. Glabe, Monoclonal antibodies against Aβ42 fibrils distinguish multiple aggregation state polymorphisms in vitro and in Alzheimer disease brain. *J. Biol. Chem.* **289**, 32131–32143 (2014).